

Analysis of stability and dual solution of MHD outer fluid velocity with partial slip on a stretching cylinder

Abstract

This manuscript discuss about the dual nature of solution, in MHD outer velocity flow, along with the stability analysis on stretching cylinder with partial slip. Differential equations are acquired by converting heat and momentum governing equations with similarity transformations. The numerical solutions of the transformed equations were computed by the Runge-Kutta Fehlberg scheme using shooting procedure. For stretching cylindrical surface, we obtained that the solution is not unique having partial slip. The dual nature of the solution exist in small range of outer velocity parameter on stretching surface. Stability analysis reveals that for lower branch (unstable solution) and upper branch (stable solution), the smallest eigenvalue is negative and positive respectively for the distinct entries of outer velocity parameter. The limit of the dual solution is $-0.03211 = \lambda_c \leq \lambda \leq \lambda_r = 0.12651$ for slip parameter, $V = 0.1$. Also, the influence of slip parameter, outer velocity parameter and magnetic parameter have been discussed on heat and flow transportation, which are presented through tables and figures.

Keywords: Partial slip, Dual solution, Stretching cylinder, MHD, Outer fluid velocity, Stability analysis.

1 Introduction

Numerous practical applications of heat and flow transportation in several divisions of manufacturing procedure lead attention of many researchers in this field of stretching surface. During these processes, sometimes the strips are stretched thereby affecting the final product.

Therefore, for researchers, study of heat and flow transportation has acquired much consideration over stretching surfaces because of their industrial applications in polymer extrusion, wire drawing and paper production etc. The impact of flow behavior over a stretched sheet was initiated by [1]. Due to wide-ranging applications of stretching material in manufacturing processes, researchers got interested in investigating the rate of transference of heat over stretching surfaces [2–5] as an extension of [1] in the field of heat transfer.

There are many physical/industrial phenomenon in which the boundary surface closely resembles cylindrical geometry. In such processes, the impact of heat and flow transportation over cylindrical stretched surfaces are essential. These processes comprise of wire drawing, hot rolling, and spinning of fibers etc. The applications of stretching surfaces in industries includes polymer extrusion process, paper production etc. Therefore, the flow characteristics over static and stretching cylinder has been initiated by [6] and [7] respectively.

Magnetic field plays a significant role in many industrial applications like petroleum refining, power generation, and cooling of objects etc. The MHD effect over a stretching cylinder has been studied in [8] and its few extensions have been reported in [9–12] with different physical conditions. These studies have confirmed that fluid velocity is strongly influenced by magnetism.

In some manufacturing processes, which involves process of filtration and controlling of heat generation, the effect of outer flow becomes significant. The effect of free stream flow on heat and mass transportation over vertical and horizontal cylinder has been studied in [13] and [14] respectively.

None of the studies cited above has reported the existence of dual solution and carried out stability analysis. The stability analysis flow solution about stagnation-point over stretching surfaces has been discussed in detail in [15–22]. Poply et al. [22] reported that the dual solution exist for stretching cylindrical surfaces.

In all of the above studies mentioned so far, the partial slip flow has not been considered. Partial slip occur when the fluid contains particulates; for example, suspensions, emulsions, polymer solutions and foams. The partial slip fluids are important in manufacturing processes, like spinning motion and filtration process. Therefore, the effect of slip velocity on stretching surfaces has been discussed by [23, 24]. The effect of slip flow on stretching cylinder in quiescent fluid has been examined in [25–29] and they reported that velocity of the fluid reduces in presence of slip surface. Critical values in slip flow in a non-Newtonian nanofluid has been reported in [30]. In unsteady flow, the flow stability for stretching/shrinking sheet with partial slip had discussed in [31] while flow stability for exponentially stretching/shrinking surface has been analyzed in [32].

The above literature survey reveals that no study had discussed so far, for stretching cylindrical surface, for calculating the flow stability in outer fluid MHD flow with partial slip. In current analysis, we investigate the same effect and results of this investigation explains that the smallest eigenvalue approaches to zero for both unstable and stable solution as the outer velocity parameter approaches to the critical point of outer velocity parameter.

2 Problem Formulation

We have considered a electrical conducting, partial slip, axisymmetric steady flow of a non-compressible fluid over stretching cylinder having constant radius a (Figure 1). The magnetic field applied radially with intensity B_o . Due to the applied magnetic field, the magnetic field which is induced being very small and that can be neglected. The stretching surface temperature $T_w(x)$ and velocity $u_w(x)$ are prescribed according to the following expressions:

$$T_w(x) = T_\infty + T_o \left(\frac{x}{l} \right)^n \quad \text{and} \quad u_w(x) = c \left(\frac{x}{l} \right).$$

Here, n be exponent of temperature. The governing equations of above considered problem are described

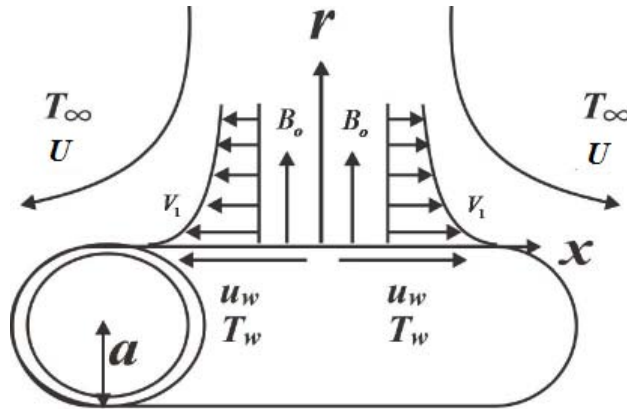


Figure 1: Schematic diagram

as:

$$\frac{\partial(ru)}{\partial x} + \frac{\partial(rv)}{\partial r} = 0 \quad (1)$$

$$u \frac{\partial u}{\partial x} + v \frac{\partial u}{\partial r} = U \frac{\partial U}{\partial x} + \frac{\nu}{r} \frac{\partial}{\partial r} \left(r \frac{\partial u}{\partial r} \right) - \frac{\sigma B_o^2}{\rho} (u - U) \quad (2)$$

$$u \frac{\partial T}{\partial x} + v \frac{\partial T}{\partial r} = \frac{\alpha}{r} \frac{\partial}{\partial r} \left(r \frac{\partial T}{\partial r} \right) \quad (3)$$

where velocity along r and x - axes are taken as v and u respectively. ν , B_o , ρ , σ , U , T and α be the kinematic viscosity, magnetic field strength, density, electrical conductivity, outer velocity, temperature and thermal diffusivity respectively.

The relevant restriction on boundary are:

$$\begin{aligned} \text{At } r = a, \quad T = T_w(x), \quad u = u_w(x) + V_o \nu \frac{\partial u}{\partial r} \quad \text{and } v = 0 \\ \text{As } r \rightarrow \infty, \quad T \rightarrow T_\infty \quad \text{and } u \rightarrow U = b \left(\frac{x}{l} \right), \end{aligned} \quad (4)$$

Here, V_o represents slip velocity.

Writing v and u in terms of $\psi(x, r)$ (stream function) as

$$v = -\frac{1}{r} \frac{\partial \psi}{\partial x} \quad \text{and} \quad u = \frac{1}{r} \frac{\partial \psi}{\partial r},$$

the continuity equation (1) is satisfied.

Introducing similarity variables

$$\eta = \frac{r^2 - a^2}{2a} \sqrt{\frac{u_w}{\nu x}}, \quad \psi = \sqrt{u_w \nu x} \, a f(\eta) \quad \text{and} \quad \theta = \frac{T - T_\infty}{T_w - T_\infty} \quad (\text{dimensionless temperature}),$$

the equations (2) and (3) are transformed as

$$(1 + 2\gamma\eta) f''' + 2\gamma f'' + f f'' - f'^2 - M(f' - \lambda) + \lambda^2 = 0 \quad (5)$$

$$(1 + 2\gamma\eta) \theta'' + 2\gamma \theta' + Pr(f\theta' - n f' \theta) = 0. \quad (6)$$

The transformed conditions on the boundary are:

$$\begin{aligned} \theta(0) = 1, \quad f'(0) = 1 + V f''(0), \quad f(0) = 0 \\ \theta(\infty) = 0, \quad f'(\infty) = \lambda \end{aligned} \quad (7)$$

where $\gamma = \frac{1}{a} \sqrt{\left(\frac{\nu l}{c}\right)}$, $V = V_o \sqrt{\frac{c l}{\nu}}$, $Pr = \frac{\nu}{\alpha}$, $\lambda = \frac{b}{c}$ and $M = \frac{\sigma B_o^2 l}{\rho c}$ represents the curvature parameter, slip parameter, Prandtl number, outer velocity parameter and magnetic parameter respectively.

The Nusselt number Nu and coefficient of skin friction C_f are described as

$$Nu = -\sqrt{Re \bar{x}} \, \theta'(0) \quad \text{and} \quad C_f = \frac{2 \bar{x} f''(0)}{\sqrt{Re}}$$

where $Re(= lc/\nu)$ represents the Reynolds number.

3 Stability Analysis

Unsteady case is considered for analyzing the flow stability and equations (2) and (3) are rewritten as:

$$\frac{\partial u}{\partial t} + u \frac{\partial u}{\partial x} + v \frac{\partial u}{\partial r} = U \frac{\partial U}{\partial x} + \frac{\nu}{r} \frac{\partial}{\partial r} \left(r \frac{\partial u}{\partial r} \right) - \frac{\sigma B_o^2}{\rho} (u - U) \quad (8)$$

$$\frac{\partial T}{\partial t} + u \frac{\partial T}{\partial x} + v \frac{\partial T}{\partial r} = \frac{\alpha}{r} \frac{\partial}{\partial r} \left(r \frac{\partial T}{\partial r} \right). \quad (9)$$

For solving the above system of equations, we add $\tau(= (\frac{c}{l}) t)$ along with η , ψ and θ as a similarity variable.

By applying similarity variables, the equations (8) and (9) are reduced to

$$(1 + 2\gamma\eta) \frac{\partial^3 f}{\partial \eta^3} + 2\gamma \frac{\partial^2 f}{\partial \eta^2} + f \frac{\partial^2 f}{\partial \eta^2} - \left(\frac{\partial f}{\partial \eta} \right)^2 - M \left(\frac{\partial f}{\partial \eta} - \lambda \right) + \lambda^2 - \frac{\partial^2 f}{\partial \eta \partial \tau} = 0 \quad (10)$$

$$(1 + 2\gamma\eta) \frac{\partial^2 \theta}{\partial \eta^2} + 2\gamma \frac{\partial \theta}{\partial \eta} + Pr \left(f \frac{\partial \theta}{\partial \eta} - n \frac{\partial f}{\partial \eta} \theta \right) - \frac{\partial \theta}{\partial \tau} = 0. \quad (11)$$

and corresponding boundary restrictions become

$$\begin{aligned} \theta(0, \tau) = 1, \quad f(0, \tau) = 0, \quad \frac{\partial f}{\partial \eta}(0, \tau) = 1 + V \frac{\partial^2 f}{\partial \eta^2}(0, \tau), \\ \theta(\infty, \tau) = 0, \quad \frac{\partial f}{\partial \eta}(\infty, \tau) = \lambda. \end{aligned} \quad (12)$$

We consider, $f(\eta) = f_0(\eta)$ and $\theta(\eta) = \theta_0(\eta)$ as a solution of equations (1)-(4), and follow the method of [33] by adopting

$$f(\eta, \tau) = f_0(\eta) + e^{-s\tau} F(\eta, \tau) \quad \text{and} \quad \theta(\eta, \tau) = \theta_0(\eta) + e^{-s\tau} G(\eta, \tau) \quad (13)$$

where s represents eigenvalue, and $F(\eta, \tau)$ and $G(\eta, \tau)$ are assumed to be insignificant in respect of $f_0(\eta)$ and $\theta_0(\eta)$. Solutions of problem (10)-(12) gives an unbounded eigenvalues as $s_1 < s_2 < \dots$. The negative and positive smallest eigenvalue indicates an initial growth and decay in the disturbance respectively and thus the flow is unstable and stable accordingly. Substituting equation (13) in equations (10)-(12), we get

$$(1 + 2\gamma\eta) \frac{\partial^3 F}{\partial \eta^3} + (2\gamma + f_0) \frac{\partial^2 F}{\partial \eta^2} + f_0'' F - (2f_0' - s + M) \left(\frac{\partial F}{\partial \eta} \right) - \frac{\partial^2 F}{\partial \eta \partial \tau} = 0 \quad (14)$$

$$(1 + 2\gamma\eta) \frac{\partial^2 G}{\partial \eta^2} + 2\gamma \frac{\partial G}{\partial \eta} + Pr [f_0 \frac{\partial G}{\partial \eta} + \theta_0' F - n(f_0' G + \theta_0 \frac{\partial F}{\partial \eta})] + sG - \frac{\partial G}{\partial \tau} = 0 \quad (15)$$

along with restrictions on the boundary are

$$\begin{aligned} F(0, \tau) = 0, \quad \frac{\partial F}{\partial \eta}(0, \tau) = V \frac{\partial^2 F}{\partial \eta^2}(0, \tau), \quad G(0, \tau) = 0 \\ \frac{\partial F}{\partial \eta}(\infty, \tau) \rightarrow 0, \quad G(\infty, \tau) \rightarrow 0. \end{aligned} \quad (16)$$

As mentioned in [16, 19], the stability of the solution is analyzed and hence $F(\eta) = F_0(\eta)$ and $G(\eta) = G_0(\eta)$ in equations (14)-(15) to check decay or growth of initial solution of equation (13). For this, linearized eigenvalue problem (17)-(18) has been solved:

$$(1 + 2\gamma\eta)F_0''' + (2\gamma + f_0)F_0'' + f_0''F_0 - (2f_0' - s + M)F_0' = 0 \quad (17)$$

$$\text{and } (1 + 2\gamma\eta)G_0'' + 2\gamma G_0' + Pr[f_0 G_0' + \theta_0' F_0 - n(f_0' G + \theta_0 F_0')] + sG = 0 \quad (18)$$

along with the restrictions on the boundary are

$$\begin{aligned} F_0(0) = 0, \quad F_0'(0) = V, \quad G_0(0) = 0 \\ F_0'(\infty) = 0, \quad G_0(\infty) = 0. \end{aligned} \quad (19)$$

For flow stability solution $f_0(\eta)$ and $\theta_0(\eta)$, it should be noted that for a fixed entry of V , Pr , γ , M and s , we determine the smallest s , suggested by [34], we solve the equations (17)-(19).

4 Results and Discussion

The boundary value problem consisting of the differential equations (5)-(6) along with boundary restrictions (7) has been computed numerically, using Runge-Kutta Fehlberg method with the shooting technique. Based on the computed results, an analysis of flow and heat transfer has been done for distinct fluid parameters. The results have been presented in terms of figures and tables.

Figure 2 shows the dual nature of the solution exists in flow transportation for $\lambda > 0$ in presence of V .

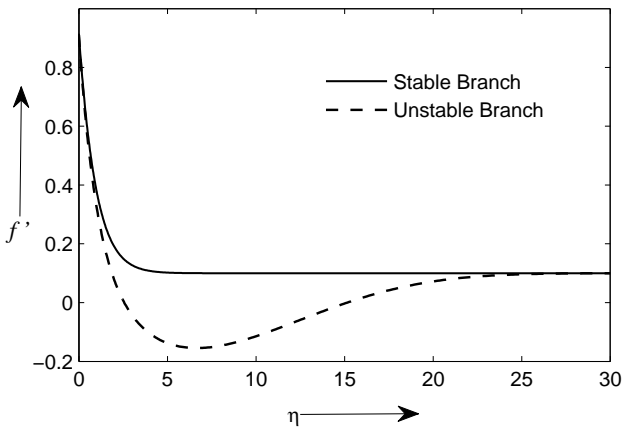


Figure 2: $f''(\eta)$ for $\lambda = 0.1$ when $V = 0.1$, $Pr = 1$, $\gamma = 0.01$, $n = 0.5$ and $M = 0.01$.

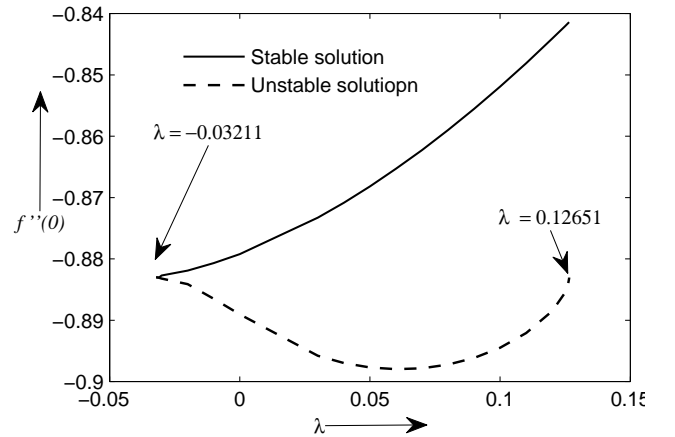


Figure 3: Variation in $f''(0)$ for distinct entries of λ when $V = 0.1$, $Pr = 1$, $\gamma = 0.01$, $n = 0.5$ and $M = 0.01$.

The upper branch (depicted by solid line) represents a stable velocity profile. On the other side, the lower

branch (depicted by dashed line) represents an unstable velocity profile. Also, the velocity profile shows an asymptotic behavior for both stable and unstable solutions (Figure 2).

Further, the limit of the unstable solution and critical point for λ has been found in the presence of slip velocity parameter $V = 0.1$. Figure 3 demonstrates the variation in $f''(0)$ against the outer velocity parameter λ in presence of slip velocity. The critical point ($\lambda_c = -0.03211$) and limit of the dual solution is $\lambda_c \leq \lambda \leq \lambda_r = 0.12651$, when $V = 0.1$, are clearly presented in Figure 3. Table 1 represents the smallest eigenvalue s for stable and unstable solution with distinct entries of outer velocity parameter λ . The results described in Table 1 explains that s has negative outcomes for unstable solution and positive for stable one. Also, the outcomes of s approaching zero when λ approaches to the critical point. Further, the analysis has been done only for the stable solution for distinct fluid parameters.

Table 1: Smallest eigenvalues s at selected entry of λ when $Pr = 1$, $\gamma = 0.01$, $n = 0.5$, $V = 0.1$ and $M = 0.01$.

λ	Upper solution	Lower solution
-0.03	0.0063	-0.0067
0	0.2016	-0.0940
0.03	0.4160	-0.1745
0.04	0.4741	-0.1979
0.05	0.5290	-0.2177
0.06	0.5821	-0.2392
0.08	0.6803	-0.2745

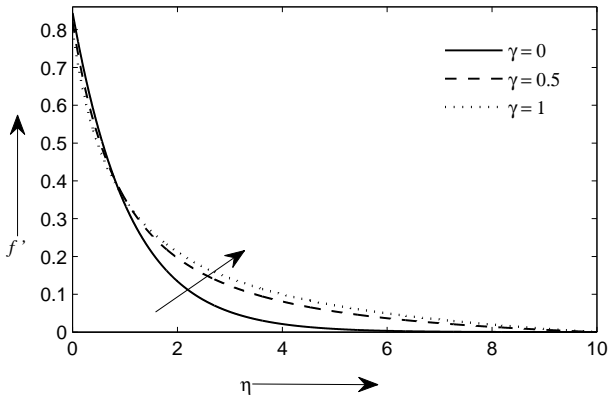


Figure 4: $f'(\eta)$ for distinct entries of γ with $V = 0.2$, when $\lambda = 0$, $Pr = 7$, $n = 0$ and $M = 0$.

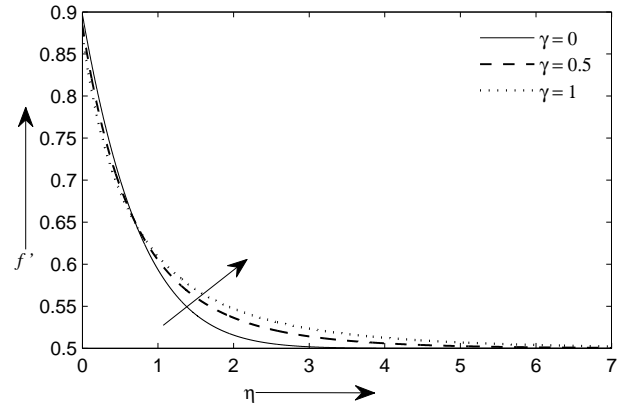


Figure 5: $f'(\eta)$ for distinct entries γ with $V = 0.2$, when $\lambda = 0.5$, $Pr = 7$, $n = 0$ and $M = 0$.

The plots of velocity profile for various entries of γ in presence of slip parameter $V = 0.2$ are shown in Figures 4, 5 and 6 for distinct entries of outer velocity parameter $\lambda = 0, 0.5$ and 2 respectively. Figures 4-5 explain that, in existence of slip velocity, fluid velocity reduces slightly with increasing γ up to a certain distance near the stretching surface and then a phase transition occurs, thereafter the fluid velocity curves show trend reversal with increase in γ . This phase transition in fluid velocity occurs with increasing γ , near the stretching surface due to the presence of slip velocity. On the other hand, for $\lambda > 1$ (Figure 6), we observed a completely opposite trend but still having a phase transition. Therefore, in all situations of ($\lambda = 0, 0.5, 2$, a transformation of stage occurs in velocity profiles which clearly demonstrates the role of slip effect near the surface.

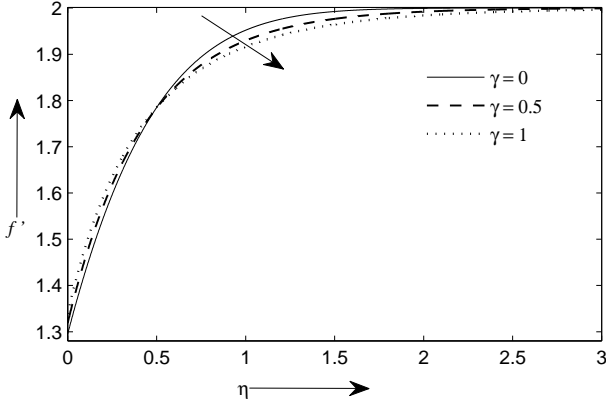


Figure 6: $f'(\eta)$ for distinct entries of γ with $V = 0.2$, when $\lambda = 2$, $Pr = 7$, $n = 0$ and $M = 0$.

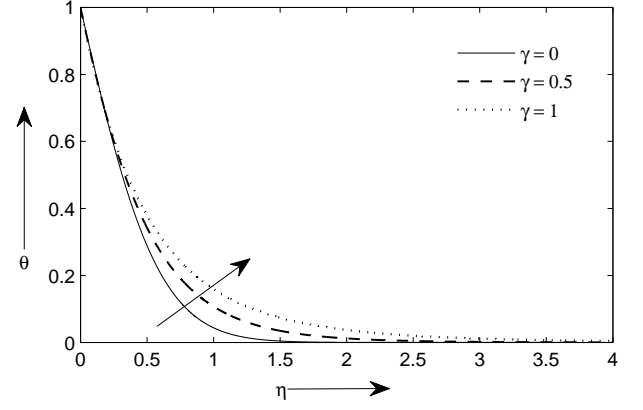


Figure 7: $\theta(\eta)$ for distinct entries of γ with $V = 0.2$, when $\lambda = 0$, $Pr = 7$, $n = 0$ and $M = 0$.

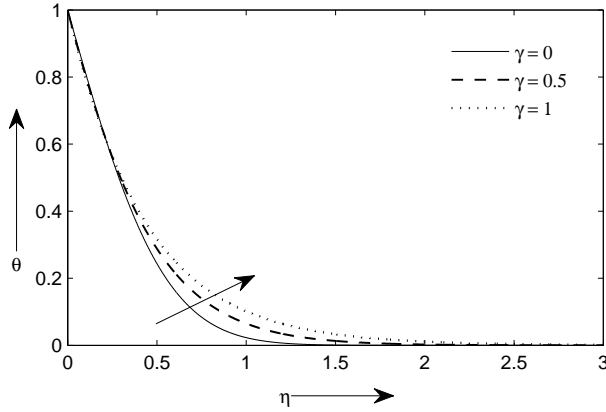


Figure 8: $\theta(\eta)$ for distinct entries of γ with $V = 0.2$, when $\lambda = 0.5$, $Pr = 7$, $n = 0$ and $M = 0$.

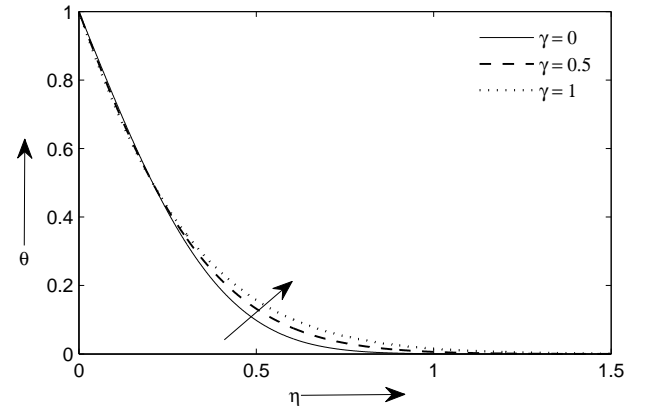


Figure 9: $\theta(\eta)$ for distinct entries of γ with $V = 0.2$, when $\lambda = 2$, $Pr = 7$, $n = 0$ and $M = 0$.

Figures 7, 8 and 9 show the effects of γ (in existence of slip velocity) on the temperature profiles for $\lambda = 0, 0.5$ and 2 respectively. In all situations, the decrease in temperature gradient is noticed. Thus, temperature rises with increasing γ . Further, we noticed that the transition point appears in all the three cases, just as in the velocity profiles (Figures 4-6).

Table 2 gives the computed outcomes of $-\theta'(0)(\propto Nu)$ and $f''(0)(\propto C_f)$ for distinct entries of γ and λ , having slip ($V = 0.2$) and no-slip ($V = 0$) condition. The $f''(0)$ values are negative for $\lambda < 1$, as it exerts a drag on the surface. The fluid velocity (Figures 4 and 5) increases for $\lambda < 1$ (after the transition point) because the value of the skin friction reduces with increasing γ whereas for $\lambda = 2$, we found a reversal trend (Figure 6) due to the opposite variations observed in the $f''(0)$. In addition, we see from Table 2 that Nu rises with increasing γ entries for each λ .

Table 2: Computed results of $f''(0)$ and $-\theta'(0)$ for distinct entries of γ when $Pr = 7$, $n = 0$ and $M = 0$.

		$V = 0$		$V = 0.2$	
λ	γ	$f''(0)$	$-\theta'(0)$	$f''(0)$	$-\theta'(0)$
0	0	-1.00001	1.89534	-0.77639	1.74198
	0.5	-1.18459	2.05619	-0.89621	1.87711
	1	-1.36386	2.21193	-1.00693	2.00717
0.5	0	-0.66726	1.98146	-0.51427	1.88983
	0.5	-0.77611	2.16816	-0.57964	2.06780
	1	-0.87584	2.35102	-0.63582	2.24329
2	0	2.01749	2.38607	1.47444	2.57343
	0.5	2.26076	2.61919	1.59258	2.81212
	1	2.48567	2.84067	1.69509	3.03840

Table 3: Computed results of $-\theta'(0)$ and $f''(0)$ for distinct entries of M when $\gamma = 0.5$, $Pr = 7$, $n = 0.5$ and $V = 0.2$.

λ	M	$-\theta'(0)$	$f''(0)$
0	0	2.47176	-0.89621
	1	2.26424	-1.17917
	2	2.11381	-1.36415
0.5	0	2.68989	-0.57964
	1	2.64240	-0.67535
	2	2.60717	-0.74758
2.0	0	3.60278	1.59258
	1	3.63188	1.69564
	2	3.65583	1.78417

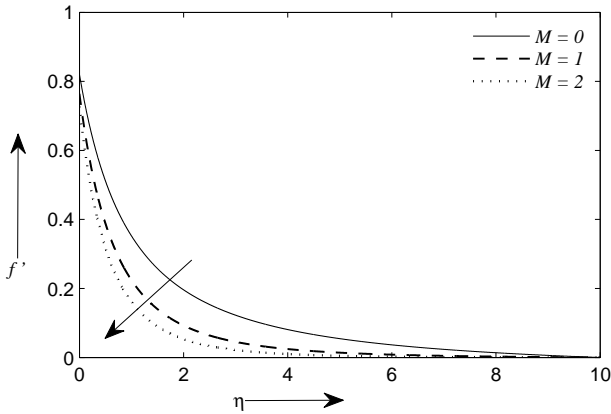


Figure 10: $f'(\eta)$ for distinct entries of M with $V = 0.2$, when $\lambda = 0$, $\gamma = 0.5$, $Pr = 7$ and $n = 0.5$.

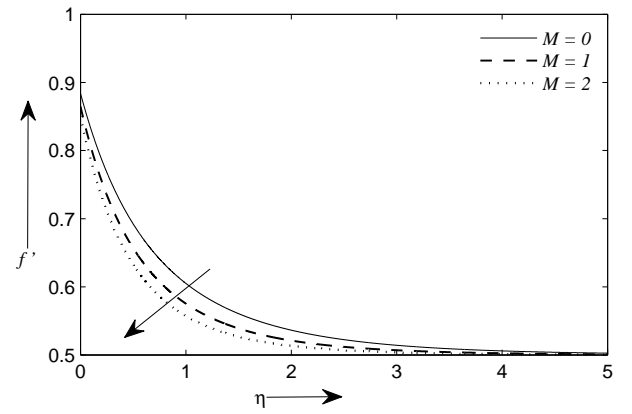


Figure 11: $f'(\eta)$ for distinct entries of M with $V = 0.2$, when $\lambda = 0.5$, $\gamma = 0.5$, $Pr = 7$ and $n = 0.5$.

Figures 10, 11 and 12 give the plots of velocity profile for $\lambda = 0$, $\lambda = 0.5$ and $\lambda = 2$ respectively for distinct entries of magnetic parameter M , with slip condition at the surface. The clear separation of curves

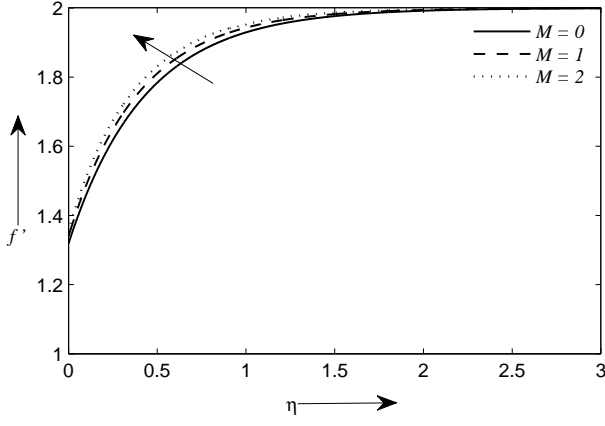


Figure 12: $f'(\eta)$ for distinct entries of M with $V = 0.2$, when $\lambda = 2$, $\gamma = 0.5$, $Pr = 7$ and $n = 0.5$.

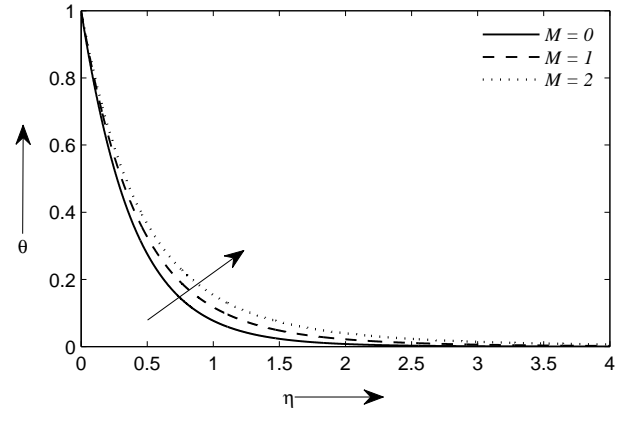


Figure 13: $\theta(\eta)$ for distinct entries of M with $V = 0.2$, when $\lambda = 0$, $\gamma = 0.5$, $Pr = 7$ and $n = 0.5$.

in each figure demonstrates the significant effect of magnetic field on the fluid flow in existence of partial slip condition. The existence of magnetic field causes a retardation in the fluid velocity (shown by the arrow in Figures 10 and 11) when $\lambda < 1$, while the impact of outer velocity dominates over magnetic impact when $\lambda > 1$, as seen from the opposite trend of velocity for $\lambda > 1$ (Figure 12).

Table 3 gives computed values of $-\theta'(0)$ and $f''(0)$ for distinct entries of M . We notice that as we increase the outer velocity parameter λ , the variation of magnetic field has a lesser effect on skin friction coefficient. The magnetic field opposes the transport phenomenon because when we increase magnetism, the Lorentz force increases and it offers large interruptions to the transport phenomenon and indirectly leads to rise in the temperature (displayed in Figure 13), as we rise the magnetic intensity. Table 3 gives the computed values of C_f and Nu for distinct entries of M in absence and presence of λ . For all λ , as we increase M the magnitude of C_f increases whereas Nu increases for $\lambda > 1$ and decreases for $\lambda < 1$.

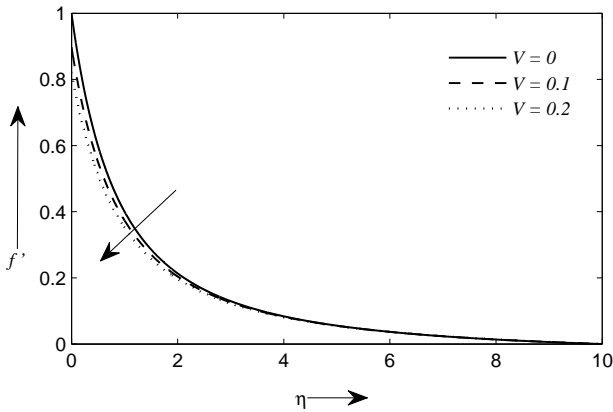


Figure 14: $f'(\eta)$ for distinct entries of V when $\lambda = 0$, $\gamma = 0.5$, $M = 0$, $n = 0$ and $Pr = 7$.

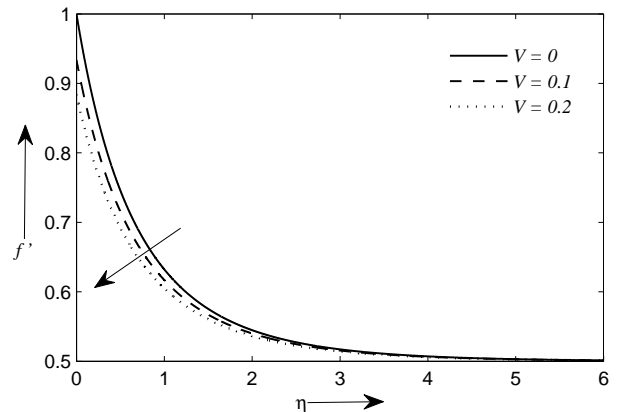


Figure 15: $f'(\eta)$ for distinct entries of V , when $\lambda = 0.5$, $\gamma = 0.5$, $M = 0$, $n = 0$ and $Pr = 7$.

Figures 14, 15 and 16 depicted curves of velocity for different entries of V for distinct λ . We observe that as V increases, there is a reduction (shown by the arrow) in velocity (Figure 14 and 15) for $\lambda < 1$, while a reverse trend is noticed for $\lambda > 1$ (Figure 16). The magnitude of velocity gradient decreases as we move away from the surface and ultimately vanishes.

Figures 17, 18 and 19 represent the temperature curves for different entries of V with different λ .

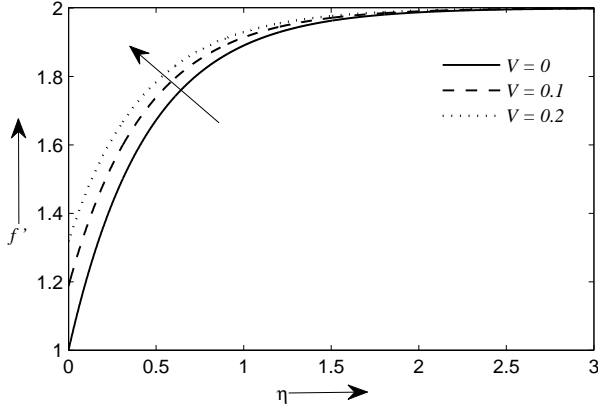


Figure 16: $f'(\eta)$ for distinct entries of V , when $\lambda = 2$, $\gamma = 0.5$, $M = 0$, $n = 0$ and $Pr = 7$.

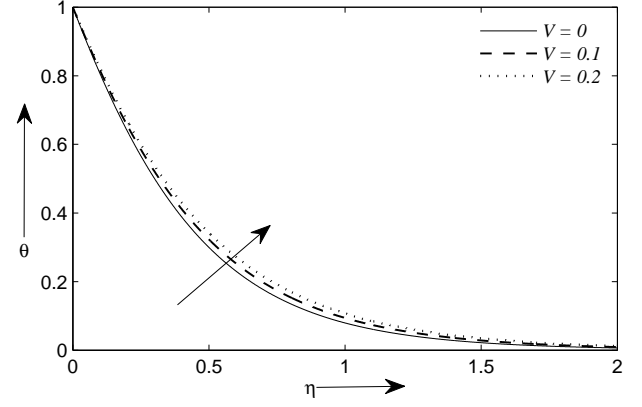


Figure 17: $\theta(\eta)$ for distinct entries of V when $\lambda = 0$, $\gamma = 0.5$, $M = 0$, $n = 0$ and $Pr = 7$.

The rise in temperature is noticed with increasing V when $\lambda < 1$ (Figures 17 and 18), while decline in temperature is noticed for $\lambda > 1$ (Figure 19).

A quick comparison of the velocity curves (Figures 14-16) and the temperature curves (Figures 17-19) showing impact of partial slip indicates that the velocity curves with greater separation are affected more by the partial slip.

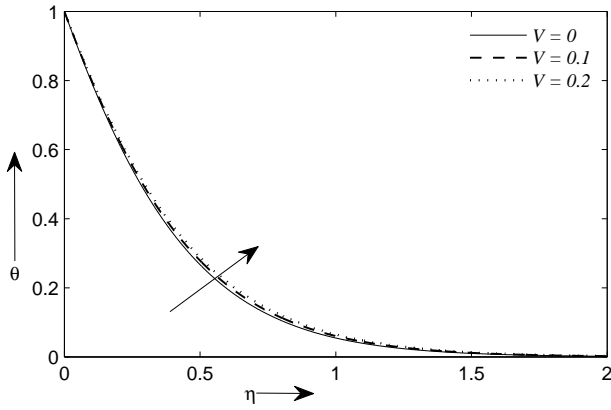


Figure 18: $\theta(\eta)$ for distinct entries of V when $\lambda = 0.5$, $\gamma = 0.5$, $M = 0$, $n = 0$ and $Pr = 7$.

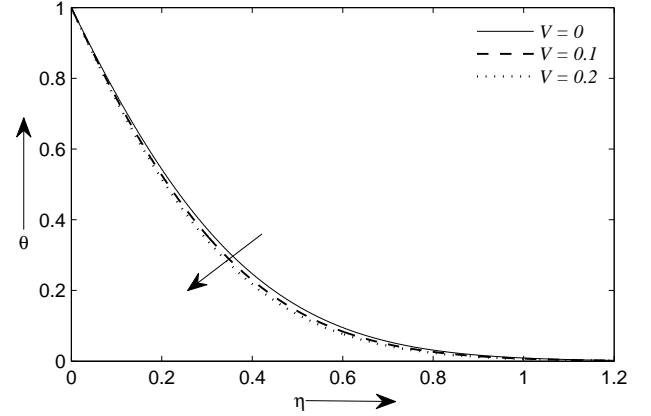


Figure 19: $\theta(\eta)$ for distinct entries of V when $\lambda = 2$, $\gamma = 0.5$, $M = 0$, $n = 0$ and $Pr = 7$.

Table 4: Computed results of $f''(0)$ and $-\theta'(0)$ for distinct entries of V when $\gamma = 0.5$, $M = 0$, $n = 0$ and $Pr = 7$.

λ	V	$f''(0)$	$-\theta'(0)$
0	0	-1.18459	2.05619
	0.1	-1.01773	1.95672
	0.2	-0.89621	1.87710
0.5	0	-0.77611	2.16815
	0.1	-0.66266	2.11132
	0.2	-0.57964	2.06780
2	0	2.26076	2.61919
	0.1	1.87383	2.73380
	0.2	1.59258	2.81212

Table 4 gives the computed values proportional to C_f and Nu for distinct V and λ . From Table 4, we noticed that with increasing V , C_f increases and Nu decreases when $\lambda < 1$. Thus friction increases which resulting a decline in velocity when $\lambda < 1$.

5 Conclusions

In this paper, we have formulated and solved numerically the heat and flow transportation problem of an MHD outer velocity flow over a progressively stretching cylinder in horizontal direction with partial slip. The key findings are:

1. Results clearly shows the existence of dual nature of the solution. Stable and unstable solution is given by upper and lower branch.
2. The limit of the unstable solution is given as $-0.03211 \leq \lambda \leq 0.12651$ for $V = 0.1$.
3. Slip effect shows a transition point in velocity profiles when we increase the curvature parameter values.
4. Smallest eigenvalue for stable solution is positive and for unstable solution is negative for different outer velocity parameter λ .

References

- [1] L. J. Crane, "Flow past a stretching plate," *Zeitschrift fr angewandte Mathematik und Physik ZAMP*, vol. 21, pp. 645–647, July 1970.
- [2] P. S. Gupta and A. S. Gupta, "Heat and mass transfer on a stretching sheet with suction or blowing," *The Canadian Journal of Chemical Engineering*, vol. 55, pp. 744–746, Dec. 1977.
- [3] M. E. Ali, "Heat transfer characteristics of a continuous stretching surface," *Wrme - und Stoffbertragung*, vol. 29, pp. 227–234, Mar. 1994.
- [4] E. M. A. Elbashbeshy and M. A. A. Bazid, "Heat transfer in a porous medium over a stretching surface with internal heat generation and suction or injection," *Appl. Math. Comput.*, vol. 158, pp. 799–807, Nov. 2004.
- [5] P. Singh, N. S. Tomer, S. Kumar, and D. Sinha, "MHD oblique stagnation-point flow towards a stretching sheet with heat transfer," *International Journal of Applied Mathematics and Mechanics*, vol. 6, no. 13, pp. 94–111, 2010.
- [6] H. Lin and Y. Shih, "Laminar boundary layer heat transfer along static and moving cylinders," *Journal of the Chinese Institute of Engineers*, vol. 3, pp. 73–79, Jan. 1980.
- [7] C. Y. Wang, "Fluid flow due to a stretching cylinder," *The Physics of Fluids*, vol. 31, pp. 466–468, Mar. 1988.

- [8] A. Ishak, R. Nazar, and I. Pop, "Magnetohydrodynamic (MHD) flow and heat transfer due to a stretching cylinder," *Energy Conversion and Management*, vol. 49, pp. 3265–3269, Nov. 2008.
- [9] K. Vajravelu, K. V. Prasad, and S. R. Santhi, "Axisymmetric magneto-hydrodynamic (MHD) flow and heat transfer at a non-isothermal stretching cylinder," *Applied Mathematics and Computation*, vol. 219, pp. 3993–4005, Dec. 2012.
- [10] R. S. Yadav and P. R. Sharma, "Effects of porous medium on MHD fluid flow along a stretching cylinder," *Annals of Pure and Applied Mathematics*, vol. 6, no. 1, pp. 104–113, 2014.
- [11] M. Y. Malik, T. Salahuddin, A. Hussain, and S. Bilal, "MHD flow of tangent hyperbolic fluid over a stretching cylinder: using Keller box method," *Journal of Magnetism and Magnetic Materials*, vol. 395, pp. 271–276, Dec. 2015.
- [12] T. Hayat, A. Shafiq, and A. Alsaedi, "MHD axisymmetric flow of third grade fluid by a stretching cylinder," *Alexandria Engineering Journal*, vol. 54, pp. 205–212, June 2015.
- [13] H. S. Takhar, A. J. Chamkha, and G. Nath, "Combined heat and mass transfer along a vertical moving cylinder with a free stream," *Heat and Mass Transfer*, vol. 36, pp. 237–246, May 2000.
- [14] Y. Y. Lok, J. H. Merkin, and I. Pop, "Mixed convection flow near the axisymmetric stagnation point on a stretching or shrinking cylinder," *International Journal of Thermal Sciences*, vol. 59, pp. 186–194, Sept. 2012.
- [15] J. Poullet and P. Weidman, "Analysis of stagnation point flow toward a stretching sheet," *International Journal of Non-Linear Mechanics*, vol. 42, pp. 1084–1091, Nov. 2007.
- [16] T. R. Mahapatra, S. K. Nandy, K. Vajravelu, and R. A. V. Gorder, "Stability analysis of fluid flow over a nonlinearly stretching sheet," *Archive of Applied Mechanics*, vol. 81, pp. 1087–1091, Aug. 2011.
- [17] T. R. Mahapatra, S. K. Nandy, K. Vajravelu, and R. A. Van Gorder, "Stability analysis of the dual solutions for stagnation-point flow over a non-linearly stretching surface," *Meccanica*, vol. 47, pp. 1623–1632, Oct. 2012.
- [18] K. Zaimi and A. Ishak, "Stagnation-point flow and heat transfer over a non-linearly stretching/shrinking sheet in a micropolar fluid," *Abstract and Applied Analysis*, vol. 2014, p. e261630, May 2014.
- [19] R. Sharma, A. Ishak, and I. Pop, "Stability analysis of magnetohydrodynamic stagnation-point flow toward a stretching/shrinking sheet," *Computers and Fluids*, vol. 102, pp. 94–98, Oct. 2014.
- [20] R. Dhanai, P. Rana, and L. Kumar, "Multiple solutions of MHD boundary layer flow and heat transfer behavior of nanofluids induced by a power-law stretching/shrinking permeable sheet with viscous dissipation," *Powder Technology*, vol. 273, pp. 62–70, Mar. 2015.
- [21] I. S. Awaludin, P. D. Weidman, and A. Ishak, "Stability analysis of stagnation-point flow over a stretching/shrinking sheet," *AIP Advances*, vol. 6, p. 045308, Apr. 2016.

- [22] V. Poply, P. Singh, and A. K. Yadav, "Stability analysis of MHD outer velocity flow on a stretching cylinder," *Alexandria Engineering Journal*, June 2017.
- [23] H. I. Andersson, "Slip flow past a stretching surface," *Acta Mechanica*, vol. 158, pp. 121–125, Mar. 2002.
- [24] P. Ariel, "Two dimensional stagnation point flow of an elastico-viscous fluid with partial slip," *ZAMM - Journal of Applied Mathematics and Mechanics / Zeitschrift fr Angewandte Mathematik und Mechanik*, vol. 88, pp. 320–324, Apr. 2008.
- [25] C. Y. Wang and C. O. Ng, "Slip flow due to a stretching cylinder," *International Journal of Non-Linear Mechanics*, vol. 46, pp. 1191–1194, Nov. 2011.
- [26] S. Mukhopadhyay, "MHD boundary layer slip flow along a stretching cylinder," *Ain Shams Engineering Journal*, vol. 4, pp. 317–324, June 2013.
- [27] M. Qasim, Z. H. Khan, W. A. Khan, and I. Ali Shah, "MHD boundary layer slip flow and heat transfer of ferrofluid along a stretching cylinder with prescribed heat flux," *PloS One*, vol. 9, no. 1, p. e83930, 2014.
- [28] N. A. A. Mat, N. M. Arifin, R. Nazar, and N. Bachok, "Boundary layer stagnation point slip flow and heat transfer towards a shrinking/stretching cylinder over a permeable surface," *Applied Mathematics*, vol. 06, pp. 466–475, Mar. 2015.
- [29] A. Majeed, T. Javed, A. Ghaffari, and M. M. Rashidi, "Analysis of heat transfer due to stretching cylinder with partial slip and prescribed heat flux: A Chebyshev Spectral Newton Iterative Scheme," *Alexandria Engineering Journal*, vol. 54, pp. 1029–1036, Dec. 2015.
- [30] R. Dhanai, P. Rana, and L. Kumar, "Critical values in slip flow and heat transfer analysis of non-Newtonian nanofluid utilizing heat source/sink and variable magnetic field: Multiple solutions," *Journal of the Taiwan Institute of Chemical Engineers*, vol. 58, pp. 155–164, Jan. 2016.
- [31] Z. Abbas, S. Rasool, and M. M. Rashidi, "Heat transfer analysis due to an unsteady stretching/shrinking cylinder with partial slip condition and suction," *Ain Shams Engineering Journal*, vol. 6, pp. 939–945, Sept. 2015.
- [32] E. H. Hafidzuddin, R. Nazar, N. M. Arifin, and I. Pop, "Boundary layer flow and heat transfer over a permeable exponentially stretching/shrinking sheet with generalized slip velocity," *Journal of Applied Fluid Mechanics*, vol. 9, no. 4, pp. 2025–2036, 2016.
- [33] J. H. Merkin, "On dual solutions occurring in mixed convection in a porous medium," *Journal of Engineering Mathematics*, vol. 20, pp. 171–179, 1985.
- [34] S. D. Harris, D. B. Ingham, and I. Pop, "Mixed convection boundary layer flow near the stagnation point on a vertical surface in a porous medium: Brinkman model with slip," *Transport Porous Media*, vol. 77, pp. 267–285, 2009.